ORIGINAL RESEARCH ARTICLE

Effects of SiO_2 and CaO on Distributions of Platinum Group Metals Between Cu–$CuO_{0.5}$ and Pb–PbO-Based Slags at 1523 K

TAKASHI MURATA and KATSUNORI YAMAGUCHI

Platinum group metals (PGMs) are recovered using molten Cu or Pb as collector metals during pyrometallurgical recycling processes. The collector metal containing PGMs is oxidized to produce a PGM-enriched alloy and slag, primarily containing Cu or Pb oxide. Additionally, the slag comprises a considerable amount of PGMs. Therefore, it is returned to the upstream processes to be used as a secondary raw material, and some of PGMs remain in the recycling processes. Herein, the distributions of Rh, Pd, and Pt between molten metals (Cu, Pb) and corresponding metal oxide-based ($CuO_{0.5}$, PbO) slags were investigated at 1523 K. SiO_2 or CaO was added to the slag to a maximum concentration of 20 mass pct, thereby reducing the oxygen partial pressure in the system. Furthermore, the addition of an optimum amount of SiO_2 or CaO into various combinations of slags and collector metals reduced the concentrations of PGMs in the slags to less than approximately 1/10 of those without adding SiO_2 or CaO. Therefore, the addition of SiO_2 or CaO during the oxidation smelting process effectively reduced the dissolution of PGMs in the slag, resulting in a less amount of PGMs circulating in the recycling processes.

https://doi.org/10.1007/s11663-023-02837-x

I. INTRODUCTION

PLATINUM group metals (PGMs) are classified as precious metals. The natural distribution of PGMs is highly concentrated in South Africa and Russia, accounting for more than 80 pct of the total production from ores.[1] Moreover, PGMs are irreplaceable for several applications owing to their unique physicochemical properties. PGM recycling technologies are expected to gain considerable significance for facilitating sustainable management and the efficient use of natural resources in future.[2,3] Automotive catalytic converters account for over 60 pct of the global demand for PGMs; therefore, the recovery of PGMs from catalytic converters is receiving significant attention worldwide. During the pyrometallurgical processes for recovering PGMs from automotive catalytic converters, the PGMs are concentrated in molten Cu or Pb, and the supporting ceramics are separated into the molten slag.[3–5] Subsequently, the molten Cu or Pb, containing PGMs, is oxidized to produce a PGM-enriched alloy and slag, which comprises primarily Cu or Pb oxide. In addition, these $CuO_{0.5}$- and PbO-based slags comprise a considerable amount of PGMs. Therefore, they are returned to the upstream processes to be used as a secondary raw material, and some of PGMs remain in the recycling processes. The prices of PGMs frequently fluctuate; therefore, they must be recovered rapidly, and the amount of PGMs circulating in the process must be reduced. Therefore, understanding the dissolution behavior of PGMs in the molten slag is essential.

The distribution behavior of PGMs between the molten metal and the slag has been reported earlier. Nakamura *et al.*[6,7] measured the solubility of Pt in various slags and suggested that Pt is stable as a platinum cation (Pt^{2+}) and platinate ion (PtO_2^{2-}) in acidic and basic slags, respectively. Wiraseranee *et al.*[8–10] and Morita *et al.*[11] determined the solubility and dissolution states of PGMs in Na_2O–SiO_2- and CaO–SiO_2-based slags. Baba *et al.*,[12] Yamaguchi,[13] Shuva *et al.*,[14] Avarmaa *et al.*,[15,16] Klemettinen *et al.*,[17] and Chen *et al.*[18,19] investigated the distribution of precious metals in a FeO_x-based slag system, which is primarily used in the smelting of non-ferrous metals. Borisov *et al.*,[20] Yamaguchi,[21] and Nisijima *et al.*[22] investigated the distribution of precious metals in an Al_2O_3–CaO–SiO_2–MgO slag system. In most of these studies, the

TAKASHI MURATA and KATSUNORI YAMAGUCHI are with the Department of Resources and Environmental Engineering, Waseda University, Building No. 60-1F-110 3-4-1 Okubo, Shinjuku-ku, Tokyo, 169-8555, Japan. Contact e-mail: tm2614971@akane.waseda.jp

Manuscript submitted December 25, 2022; accepted May 30, 2023. Article published online June 26, 2023.

distributions of precious metals to the slag are demonstrated an increase in the dissolution of PGMs in slags with increasing oxygen partial pressure and concentration of Cu in slags. We investigated the distribution of Pt between the molten Cu and the SiO_2–CaO–CrO_x slag system in our previous study[23] and observed an increase in the dissolution of Pt in the slag with increasing concentration of Cr in the slag. Swinbourne *et al.*[24] investigated the dissolution of Au in PbO–SiO_2 slag and reported that the Au concentration increased with increasing PbO concentration in the slag. However, to the best of our knowledge, the distribution of PGMs in $CuO_{0.5}$- or PbO-based slags has not been reported yet. Understanding the distribution behavior of PGMs in slags is important for the effective recycling of PGMs using the oxidation smelting process.

In this study, the distributions of Rh, Pd, and Pt between molten metals (Cu and Pb) and their corresponding metal oxide-based ($CuO_{0.5}$ and PbO) slags were investigated at 1523 K by adding SiO_2 or CaO to the slags to a maximum concentration of 20 mass pct.

II. EXPERIMENTAL PROCEDURE

A total of 6 g of $CuO_{0.5}$ (99 mass pct purity), SiO_2 (99.9 mass pct purity), and CaO (99.9 mass pct purity) powder as a slag and 4 g of the homogenized 91 mass pct Cu and 3 mass pct of Rh, Pd, and Pt alloy were put into a MgO crucible with an inner diameter, a height, and a wall thickness of 18, 40, and 2.5 mm, respectively. In addition, a total of 9 g of PbO (99.9 mass pct purity), SiO_2, and CaO powder as slag and 6 g of the homogenized 97.06 mass pct Pb and 0.9814 mass pct of Rh, Pd, and Pt alloy were placed in a MgO crucible of the same dimensions as mentioned above. Different total masses were used to ensure the volume required for the measurement of the oxygen partial pressure. Furthermore, different alloy compositions were used to ensure equal mole fractions of PGMs in the Cu and Pb-based systems. Subsequently, the sample was injected into a mullite reaction tube with an Ar (99.99 vol pct purity) gas flow rate of 200 mL/min. After holding the sample at 1523 K (± 3 K) in a furnace using SiC-heating elements for 4 h, the oxygen partial pressure was indirectly measured *via* an oxygen-concentration cell using an MgO-stabilized ZrO_2 solid electrolyte, with the following formula [1]:

$$+\mathrm{Pt/Ni \cdot NiO/ZrO_2 \cdot MgO/sample/Re/Pt} - . \quad [1]$$

Both electrodes were immersed in the slag and alloy phase. The change in the potential difference between 1 min was confirmed to be less than 0.005 V (±0.03 in terms of $\log p_{O_2}$). Even when the Ar gas supply was temporarily stopped, the same potential difference was measured as when the gas was supplied. Therefore, it is considered that this measurement was not affected by the impurity oxygen in the Ar gas. The sample was held for another 0.5 h and quenched with water. A schematic of the experimental setup is shown in Figure 1. Subsequently, the slag and alloy phases in the crucible were separated and dissolved in an acid. The concentrations of the slag and alloy phases were quantified using inductively coupled plasma optical emission spectrometry (ICP-OES) and inductively coupled plasma mass spectrometry (ICP-MS). Tables I and II list the initial slag compositions and experimental results for the Cu–$CuO_{0.5}$ and Pb–PbO systems. The maximum amount of SiO_2 or CaO added was determined based on the binary state diagram of the respective slag system.[25–28] The respective binary phase diagrams for slags are shown in Figure 2. Although MgO dissolves in the slag after equilibration, preliminary experiments confirmed that it is a homogeneous liquid.

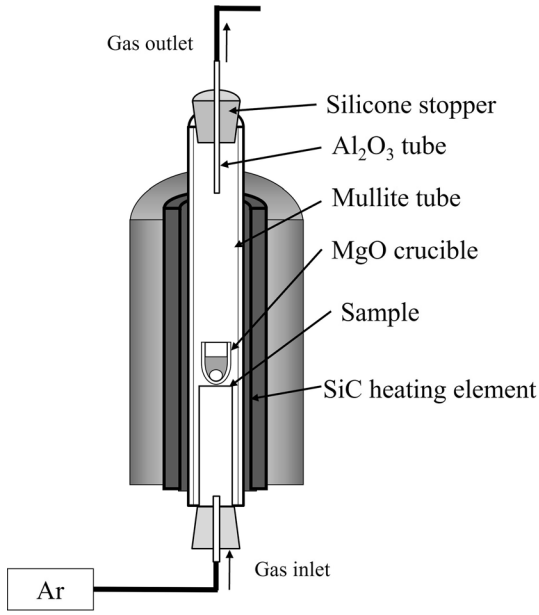

Fig. 1—Schematic of the experimental setup.

To confirm whether equilibrium was sufficiently reached with a holding time of 4 h, experiments were conducted with 100 mass pct $CuO_{0.5}$ slag for 10 h and 24 h. The same results were obtained in both experiments, indicating that equilibrium was reached by holding the slag for 4 h.

III. RESULTS AND DISCUSSION

A. *Solubility of MgO in Slags*

The MgO crucible was partially dissolved in the slag and equilibrated. Figure 3 shows the relationship between the concentration of MgO and the concentration of SiO_2 or CaO in the slag. MgO barely dissolves, with a maximum of 0.34 mass pct, in the $CuO_{0.5}$, $CuO_{0.5}$–CaO, PbO, and PbO–CaO slags. In contrast, a significant increase in the MgO concentration is observed with increasing concentration of SiO_2 in the $CuO_{0.5}$–SiO_2 and PbO–SiO_2 slags. This is because MgO and CaO are basic oxides, and SiO_2 is an acidic oxide. Therefore, the use of CaO is speculated to suppress the reduction in the service life of the furnace refractory if the refractory is a basic oxide.

Table I. Experimental Results for the Cu–$CuO_{0.5}$ System at 1523 K

		Initial Slag Composition (Mass Pct)			Concentration in Slag Phase (Mass Pct)							Concentration in Alloy Phase (Mass Pct)					Distribution Ratio of PGMs: $L_X^{s/m}$		
No.	Time (h)	$CuO_{0.5}$	SiO_2	CaO	$CuO_{0.5}$	SiO_2	CaO	MgO	Rh	Pd	Pt	Cu	Rh	Pd	Pt	$\log p_{O_2}$	Rh	Pd	Pt
1	4	100	—	—	99.7	—	—	0.178	0.035	0.070	0.028	91.4	2.83	3.05	2.67	− 3.77	0.012	0.023	0.011
2	10	100	—	—	99.7	—	—	0.198	0.033	0.068	0.029	91.6	2.78	2.89	2.72	− 3.74	0.012	0.024	0.011
3	24	100	—	—	99.7	—	—	0.201	0.034	0.074	0.029	91.4	2.88	2.95	2.77	− 3.75	0.012	0.025	0.010
4	4	95	5	—	94.1	4.97	—	0.897	0.0088	0.015	0.0054	92.0	2.66	2.82	2.54	− 3.79	0.0033	0.0054	0.0021
5	4	90	10	—	87.3	9.59	—	3.10	0.0023	0.0043	0.0017	92.1	2.63	2.77	2.47	− 3.84	0.00086	0.0016	0.00068
6	4	95	—	5	94.2	—	5.50	0.296	0.0044	0.0062	0.0023	92.0	2.66	2.88	2.50	− 4.20	0.0017	0.0022	0.00093
7	4	90	—	10	89.3	—	10.3	0.342	0.0037	0.0038	0.00079	91.8	2.73	2.92	2.56	− 4.27	0.0014	0.0013	0.00031

Table II. Experimental Results for the Pb–PbO System at 1523 K

		Initial Slag Composition (Mass Pct)			Concentration in Slag Phase (Mass Pct)							Concentration in Alloy Phase (Mass Pct)					Distribution Ratio of PGMs: $L_X^{s/m}$		
No.	Time (h)	PbO	SiO_2	CaO	PbO	SiO_2	CaO	MgO	Rh	Pd	Pt	Pb	Rh	Pd	Pt	$\log p_{O_2}$	Rh	Pd	Pt
8	4	100	—	—	99.8	—	—	0.234	0.0033	0.0018	0.0019	96.5	1.03	1.24	1.20	− 5.32	0.0032	0.0015	0.0015
9	4	95	5	—	94.4	4.34	—	1.23	0.0019	0.00044	0.00035	96.4	1.10	1.25	1.21	− 5.54	0.0018	0.00036	0.00029
10	4	90	10	—	87.2	10.8	—	2.04	0.0013	0.000051	0.000093	95.9	1.30	1.36	1.47	− 6.08	0.0010	0.000037	0.000063
11	4	85	15	—	82.5	15.1	—	2.40	0.00058	0.000034	0.000044	96.6	1.01	1.21	1.21	− 6.46	0.00057	0.000028	0.000037
12	4	80	20	—	77.3	18.7	—	4.00	0.0011	0.000026	0.000039	96.2	1.19	1.28	1.32	− 6.54	0.00093	0.000021	0.000030
13	4	95	—	5	94.8	—	4.97	0.238	0.0013	0.00082	0.00018	96.5	1.08	1.19	1.22	− 5.53	0.0012	0.00069	0.00015

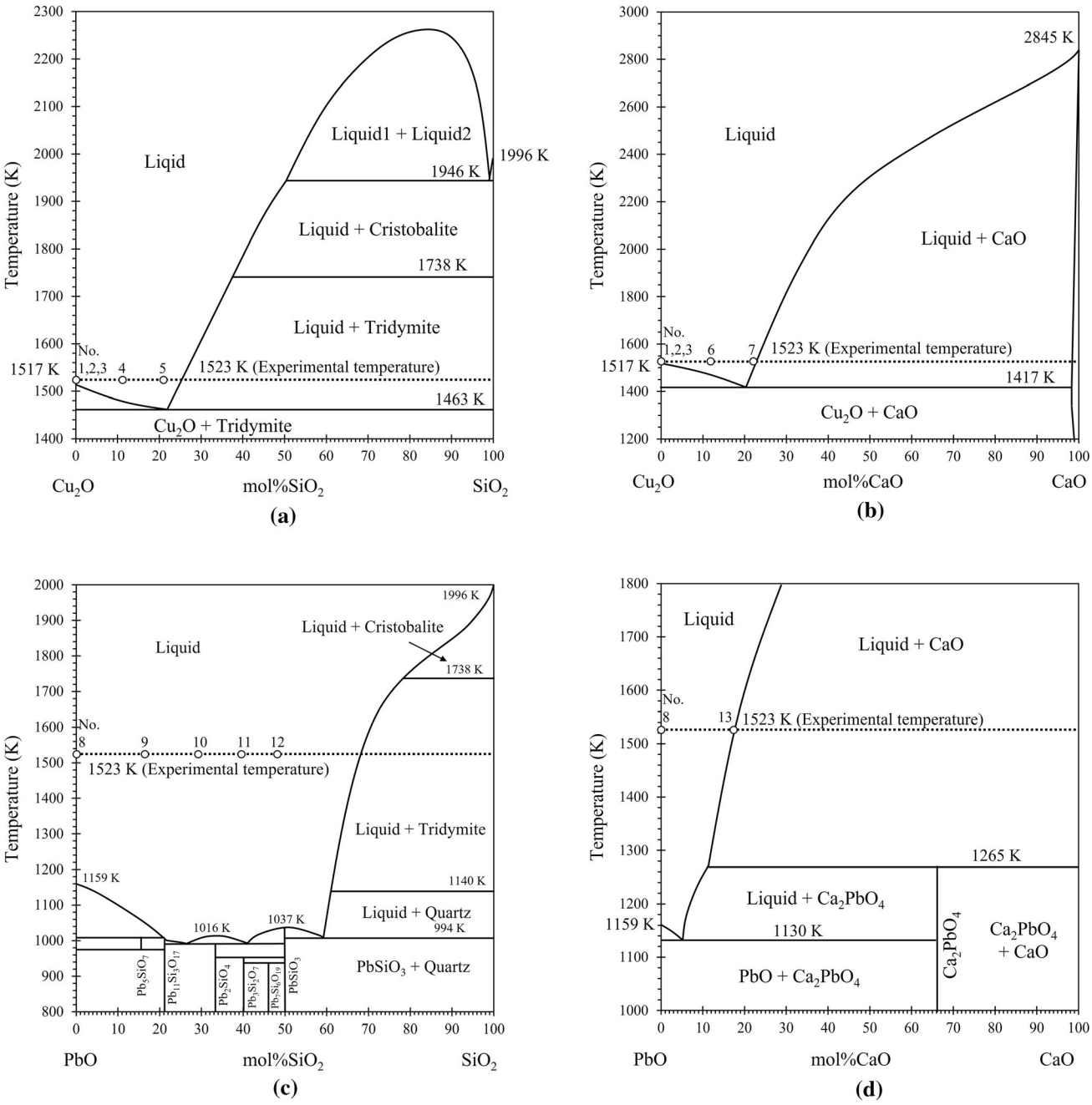

Fig. 2—Binary phase diagrams: (*a*) Cu_2O–SiO_2, (*b*) Cu_2O–CaO, (*c*) PbO–SiO_2, and (*d*) PbO–CaO.[25–28]

B. *Oxygen Partial Pressure*

The oxygen partial pressure in the system was indirectly measured *via* an oxygen-concentration cell using a MgO-stabilized ZrO_2 solid electrolyte. Figure 4 shows the relationship between the oxygen partial pressure and the concentration of SiO_2 or CaO in the slags.

The dashed line in Figure 4 represents the oxygen partial pressure ($\log p_{O_2} = -3.82, -5.33$), calculated using the standard Gibbs free energy change for reactions of [2] and [3] in the SGPS database of the thermodynamic computing system FactSage ver.8.1,[29] when the pure liquid Cu and $CuO_{0.5}$ and the pure liquid Pb and PbO are in equilibrium at 1523 K, respectively. The oxygen partial pressure at equilibrium without SiO_2 or CaO agrees well with the calculated value. Furthermore, the oxygen partial pressure with the addition of CaO in the Cu-based system is lower than that with the addition of SiO_2. The oxygen partial pressure decreased with increasing concentration of SiO_2 in the Cu-based system. This is because the SiO_2 and CaO change the activities of $CuO_{0.5}$ and PbO. The validity of this result is discussed in *Activity coefficients* of section D.

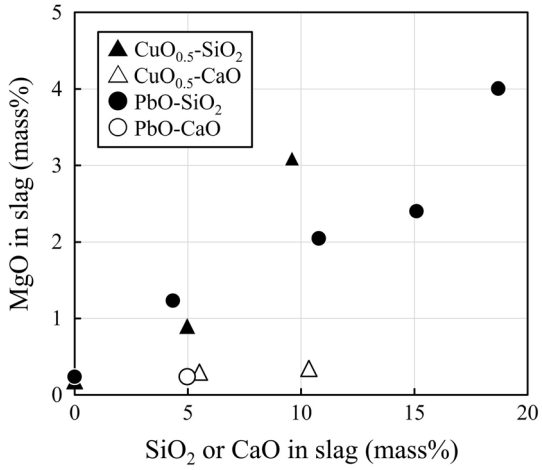

Fig. 3—Solubility of MgO in the slag at 1523 K.

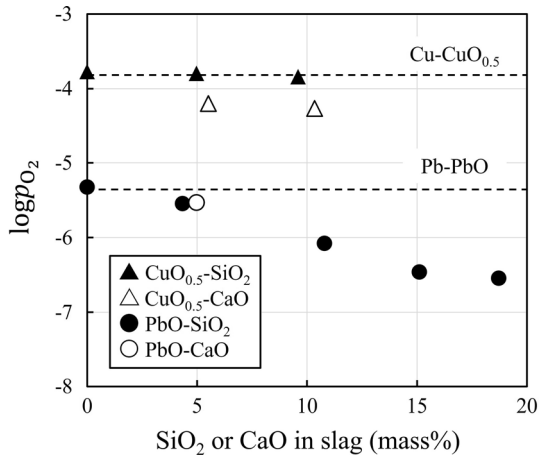

Fig. 4—Relationship between the oxygen partial pressure and the concentration of SiO_2 or CaO in the slags.

$$4\text{Cu (l)} + \text{O}_2\text{(g)} = 4\text{CuO}_{0.5}\text{(l)}: \ \Delta G^0 = -111311\text{(J) at 1523 K}^{[29]}, \quad [2]$$

$$2\text{Pb (l)} + \text{O}_2\text{(g)} = 2\text{PbO (l)}: \Delta G^0 = -155332\text{(J) at 1523 K}^{[29]}. \quad [3]$$

C. *Distributions of Rh, Pd, and Pt in the Alloy and Slag*

The distribution ratios of Rh, Pd, and Pt between the slag and alloy were defined using Eq. [4]:

$$L_{\text{X}}^{\text{s/m}} = \frac{(\text{X (mass pct) in Slag})}{(\text{X (mass pct) in Alloy})}, \quad [4]$$

where X = Rh, Pd, or Pt. Figures 5 and 6 depict the relationship between the distribution ratios of PGMs and the concentrations of SiO_2 or CaO in the $CuO_{0.5}$- and PbO-based slags, respectively.

The addition of SiO_2 or CaO (approximately 10 mass pct) to the Cu-based system decreases the distribution ratios of all PGMs to less than 1/10 of those without SiO_2 or CaO. Similarly, the addition of SiO_2 or CaO to the Pb-based system decreases the distribution ratios of all PGMs. Therefore, the addition of CaO or SiO_2 in the slag is suitable for reducing the dissolution of PGMs in the slag during the oxidation smelting process.

D. *Activity Coefficient*

The activity coefficients of each component in the slag were calculated to understand the interactions of each component. The activities used in this study were in the Raoult law standard state. The estimation of the activity of each component in the metal alloy requires thermodynamic data for the Cu–Rh–Pd–Pt and Pb–Rh–Pd–Pt systems; however, such thermodynamic data have not been measured. Therefore, the activities were considered consistent with the mole fractions based on the Rawls rule. The mole fractions of Cu and Pb were higher than 0.92; therefore, the activity coefficients $\gamma_{\text{Pb(l)}}$ and $\gamma_{\text{Cu(l)}}$ were assumed to be equal to one.

The activity coefficients of $CuO_{0.5}$ and PbO in the slag were calculated. The changes in standard Gibbs free energy (ΔG^0) for the oxidation reactions of Cu and Pb are presented in Eqs. [2] and [3]. At equilibrium, the relationship between ΔG^0 and the activity of Cu or Pb is expressed by Eqs. [5] and [6], respectively:

$$\Delta G_{[2]}^0 = -\text{R}T\ln\frac{a_{\text{CuO}_{0.5}\text{(l)}}^4}{a_{\text{Cu(l)}}^4 \cdot p_{\text{O}_2}}, \quad [5]$$

$$\Delta G_{[3]}^0 = -\text{R}T\ln\frac{a_{\text{PbO(l)}}^2}{a_{\text{Pb(l)}}^2 \cdot p_{\text{O}_2}}, \quad [6]$$

where ΔG^0 is the change in the standard Gibbs free energy of reactions [2] and [3], R is the gas constant, T is the absolute temperature, a_{i} is the activity of component i, and p_{O_2} is the oxygen partial pressure. The activity a_{i} is expressed by Eq. [7]:

$$a_{\text{i}} = \gamma_{\text{i}} \cdot x_{\text{i}}, \quad [7]$$

where γ_{i} is the activity coefficient, and x_{i} is the molar fraction of component i. The activity coefficients of the liquid $CuO_{0.5}$ ($\gamma_{\text{CuO}_{0.5}\text{(l)}}$) and PbO ($\gamma_{\text{PbO(l)}}$) in the slag can be calculated using Eqs. [8] and [9], respectively:

$$\gamma_{\text{CuO}_{0.5}\text{(l)}} = \frac{1}{x_{\text{CuO}_{0.5}}} \cdot \left\{ x_{\text{Cu}}^4 \cdot p_{\text{O}_2} \cdot \exp\left(\frac{-\Delta G_{[2]}^0}{\text{R}T}\right)\right\}^{\frac{1}{4}}, \quad [8]$$

$$\gamma_{\text{PbO(l)}} = \frac{1}{x_{\text{PbO}}} \cdot \left\{ x_{\text{Pb}}^2 \cdot p_{\text{O}_2} \cdot \exp\left(\frac{-\Delta G_{[3]}^0}{\text{R}T}\right)\right\}^{\frac{1}{2}}. \quad [9]$$

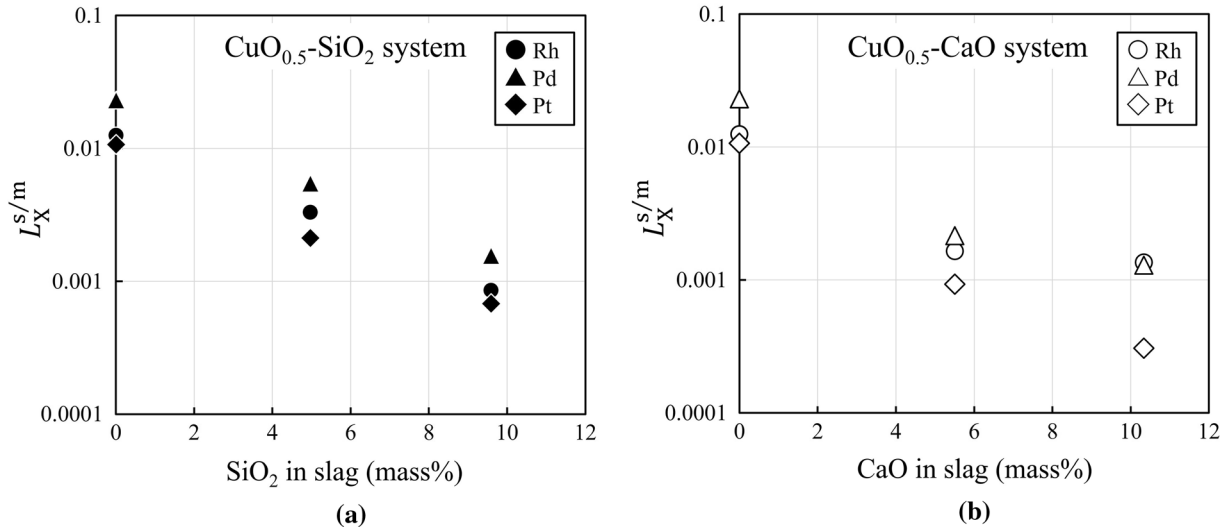

Fig. 5—Distribution ratios of Rh, Pd, and Pt between liquid Cu and $CuO_{0.5}$-based slag at 1523 K: (*a*) $CuO_{0.5}$–SiO_2 slag system and (*b*) $CuO_{0.5}$–CaO slag system.

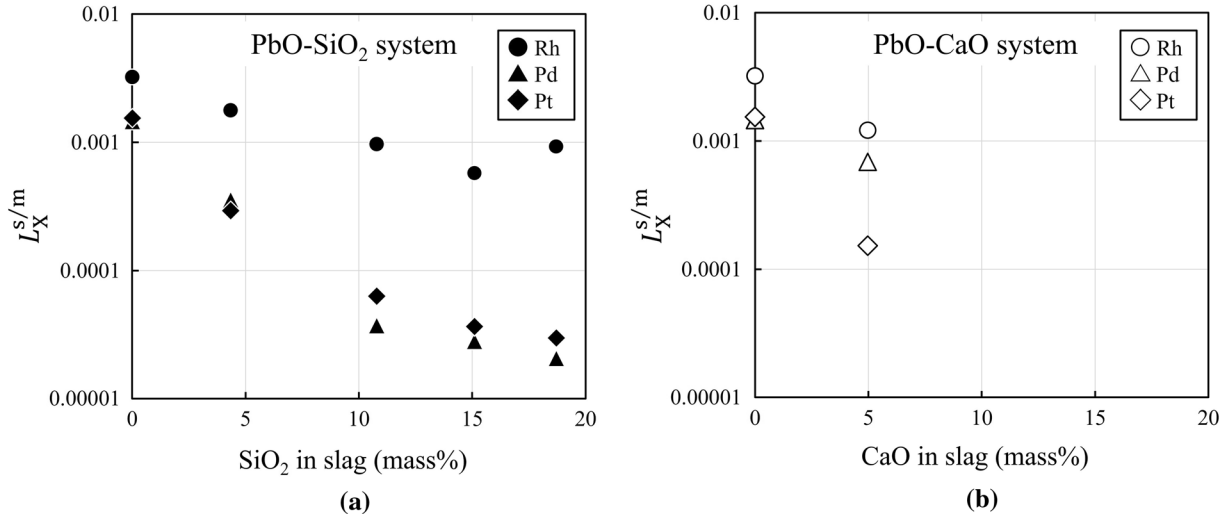

Fig. 6—Distribution ratios of Rh, Pd, and Pt between liquid Pb and PbO-based slag at 1523 K: (*a*) PbO–SiO_2 slag system and (*b*) PbO–CaO slag system.

Further, the activity coefficients of the PGM oxides in the slag were calculated. The interactions between PGMs were assumed negligible in each phase. Moreover, the oxidation states of the PGMs in the slag could not be determined. Therefore, considering the reactions of PGM oxides described in the thermodynamic database HSC ver.6.1,[30] we assumed that PGMs dissolve in the slag as $RhO_{1.5}$, PdO, and PtO_2. ΔG^0 for the oxidation reactions of Rh, Pd, and Pt are presented in Eqs. [10] through [12]. The thermodynamic database HSC provides data without any distinction between solid and liquid; therefore, all the metals and their corresponding oxides were assumed solids.

$$\frac{4}{3}\mathrm{Rh\ (s)} + \mathrm{O_2(g)} = \frac{4}{3}\mathrm{RhO_{1.5}(s)}:\ \Delta G^0 = 16839(\mathrm{J})\ \text{at}\ 1523\ \mathrm{K}^{[30]}, \quad [10]$$

$$2\mathrm{Pd\ (s)} + \mathrm{O_2(g)} = 2\mathrm{PdO\ (s)}:\ \Delta G^0 = 87898(\mathrm{J})\ \text{at}\ 1523\ \mathrm{K}^{[30]}, \quad [11]$$

$$\mathrm{Pt\ (s)} + \mathrm{O_2(g)} = \mathrm{PtO_2(s)}:\ \Delta G^0 = 100265\ (\mathrm{J})\ \text{at}\ 1523\ \mathrm{K}^{[30]}. \quad [12]$$

The values of activity coefficients at infinite dilution for binary systems, adopted from the SGnobl values from FactSage ver.8.1, were used as the activity coefficients of Rh, Pd, and Pt in molten Cu and Pb.[29] Table III lists the activity coefficient at infinite dilution in binary systems at 1523 K. The activity coefficients of PGM oxides in the slag were calculated using Eqs. [13] through [15] in the same manner as those of Cu and Pb:

$$\gamma_{RhO_{1.5}(s)} = \frac{1}{x_{RhO_{1.5}}} \cdot \left\{ a_{Rh(s)}^{\frac{4}{3}} \cdot p_{O_2} \cdot \exp\left(\frac{-\Delta G^0_{[10]}}{RT}\right) \right\}^{\frac{3}{4}}, \quad [13]$$

$$\gamma_{PdO(s)} = \frac{1}{x_{PdO}} \cdot \left\{ a_{Pd(s)}^{2} \cdot p_{O_2} \cdot \exp\left(\frac{-\Delta G^0_{[11]}}{RT}\right) \right\}^{\frac{1}{2}}, \quad [14]$$

$$\gamma_{PtO_2(s)} = \frac{1}{x_{PtO_2}} \cdot \left\{ a_{Pt(s)} \cdot p_{O_2} \cdot \exp\left(\frac{-\Delta G^0_{[12]}}{RT}\right) \right\}. \quad [15]$$

Table III. Activity Coefficient at Infinite Dilution in Binary Systems at 1523 K[29]

Phase	$\gamma^0_{Rh(s)}$	$\gamma^0_{Pd(s)}$	$\gamma^0_{Pt(s)}$
Cu	7.68	0.0364	0.0980
Pb	0.203	0.0279	1.37

The PGM oxides are calculated as solids because thermodynamic data for liquids are not available. Tables IV and V list the calculated activity and activity coefficient of each oxide. Figures 7 and 8 depict the relationship between the activity and the molar fraction in the slag of the Cu–$CuO_{0.5}$ and Pb–PbO systems, respectively.

Takeda *et al.*[31] reported the activity of $CuO_{0.5}$ under MgO saturation at 1523 K for the $CuO_{0.5}$–SiO_2 system. Okajima *et al.*[32] reported the activity of PbO at 1323 K for the PbO–CaO system. For the PbO–CaO system, experimental data could not be found, but solution

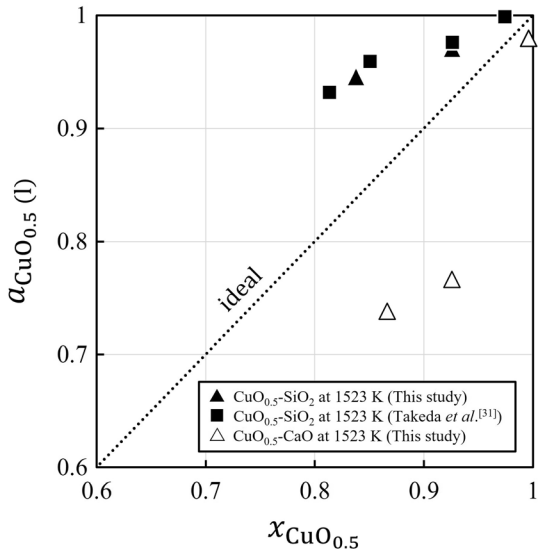

Fig. 7—Relationship between the activity and the mole fraction of $CuO_{0.5}$ in the $CuO_{0.5}$–SiO_2 and $CuO_{0.5}$–CaO systems.

Table IV. Activity and Activity Coefficient of the Cu–$CuO_{0.5}$ System at 1523 K

No.	$a_{CuO_{0.5}(l)}$	$\gamma_{CuO_{0.5}(l)}$	$a_{RhO_{1.5}(s)}$	$\gamma_{RhO_{1.5}(s)}$	$a_{PdO(s)}$	$\gamma_{PdO(s)}$	$a_{PtO_2(s)}$	$\gamma_{PtO_2(s)}$
1	0.980	0.984	7.7×10^{-5}	0.31	2.8×10^{-7}	5.9×10^{-4}	5.5×10^{-11}	5.2×10^{-7}
4	0.970	1.05	6.9×10^{-5}	1.1	2.5×10^{-7}	2.5×10^{-3}	4.9×10^{-11}	2.5×10^{-6}
5	0.945	1.13	6.3×10^{-5}	4.2	2.3×10^{-7}	8.4×10^{-3}	4.3×10^{-11}	7.3×10^{-6}
6	0.766	0.828	3.4×10^{-5}	1.1	1.6×10^{-7}	3.9×10^{-3}	1.9×10^{-11}	2.3×10^{-6}
7	0.738	0.852	3.1×10^{-5}	1.3	1.5×10^{-7}	6.1×10^{-3}	1.7×10^{-11}	6.0×10^{-6}

Table V. Activity and Activity Coefficient of the Pb–PbO System at 1523 K

No.	$a_{PbO(l)}$	$\gamma_{PbO(l)}$	$a_{RhO_{1.5}(s)}$	$\gamma_{RhO_{1.5}(s)}$	$a_{PdO(s)}$	$\gamma_{PdO(s)}$	$a_{PtO_2(s)}$	$\gamma_{PtO_2(s)}$
8	0.953	0.966	1.6×10^{-7}	2.2×10^{-3}	4.5×10^{-8}	1.2×10^{-3}	3.0×10^{-11}	1.4×10^{-6}
9	0.734	0.913	1.1×10^{-7}	3.1×10^{-3}	3.5×10^{-8}	4.4×10^{-3}	1.8×10^{-11}	5.2×10^{-6}
10	0.393	0.625	5.3×10^{-8}	2.7×10^{-3}	2.0×10^{-8}	2.7×10^{-2}	6.3×10^{-12}	8.3×10^{-6}
11	0.256	0.471	2.1×10^{-8}	2.6×10^{-3}	1.2×10^{-8}	2.5×10^{-2}	2.2×10^{-12}	6.5×10^{-6}
12	0.055	0.120	2.5×10^{-9}	1.8×10^{-4}	2.7×10^{-9}	8.1×10^{-3}	1.1×10^{-13}	4.1×10^{-7}
13	0.749	0.916	1.1×10^{-7}	4.6×10^{-3}	3.4×10^{-8}	2.3×10^{-3}	1.9×10^{-11}	1.0×10^{-5}

thermodynamic data are available in FToxid in FactSage ver. 8.1.[29] The results obtained in this study are in agreement with those in the aforementioned literature.[29,31,32] The interaction between $CuO_{0.5}$ and SiO_2 is considered repulsive owing to the positively biased activity of $CuO_{0.5}$ in the $CuO_{0.5}$–SiO_2 system from the ideal value. In contrast, an attractive interaction is observed between $CuO_{0.5}$ and PbO because of their negatively biased activity in the $CuO_{0.5}$–CaO, PbO–SiO_2, and PbO–CaO systems.

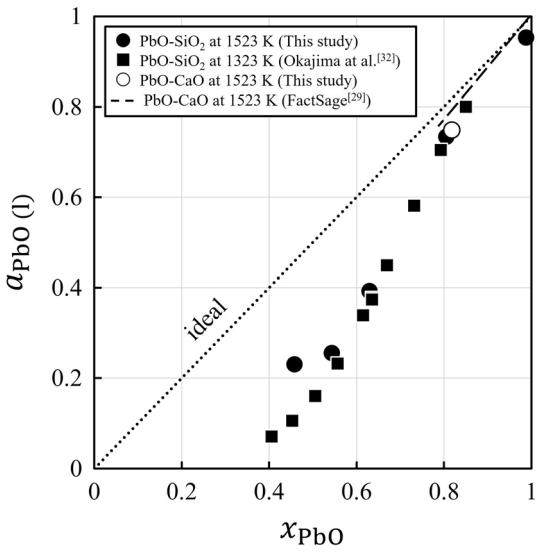

Fig. 8—Relationship between the activity and the mole fraction of PbO in the PbO–SiO_2 and PbO–CaO systems.

Figures 9, 10, and 11 depict the activity of $RhO_{1.5}$, PdO, and PtO_2, respectively, as a function of the molar fraction of $CuO_{0.5}$ and PbO in the slags of the Cu–$CuO_{0.5}$ and Pb–PbO systems. The PGMs are speculated to be completely dissolved in the slag in the form of $RhO_{1.5}$, PdO, and PtO_2. In all combinations except for $RhO_{1.5}$ in the PbO–SiO_2 system, the activity coefficient of the PGM oxides increased with the coexistence of SiO_2 or CaO. This suggests that these PGM oxides are repulsive to SiO_2 and CaO in the slag.

IV. CONCLUSIONS

The distribution behavior of Rh, Pd, and Pt during the oxidation smelting process was investigated for the recovery of PGMs. The effects of SiO_2 and CaO on the distributions of Rh, Pd, and Pt in the Cu–$CuO_{0.5}$ and Pb–PbO systems were investigated. The major conclusions are as follows:

1. MgO barely dissolved (a maximum of 0.34 mass pct) in the $CuO_{0.5}$, $CuO_{0.5}$–CaO, PbO, and PbO–CaO slags. In contrast, dissolution of MgO increased with increasing concentration of SiO_2 in the $CuO_{0.5}$–SiO_2 and PbO–SiO_2 slags.
2. The addition of SiO_2 or CaO reduced the oxygen partial pressure in the system. Furthermore, for all combinations of slag systems and PGMs, the addition of an optimum amount of SiO_2 or CaO reduced the concentrations of PGMs in the slags to less than approximately 1/10 of that without adding SiO_2 or CaO. The tendency for PGMs dissolved in the slags to increase with increasing oxygen partial pressure [6,8,12–14,16,22] and with increasing concentrations of Cu or Pb in the slags[12,13,16,22,24] is consistent with previous studies.

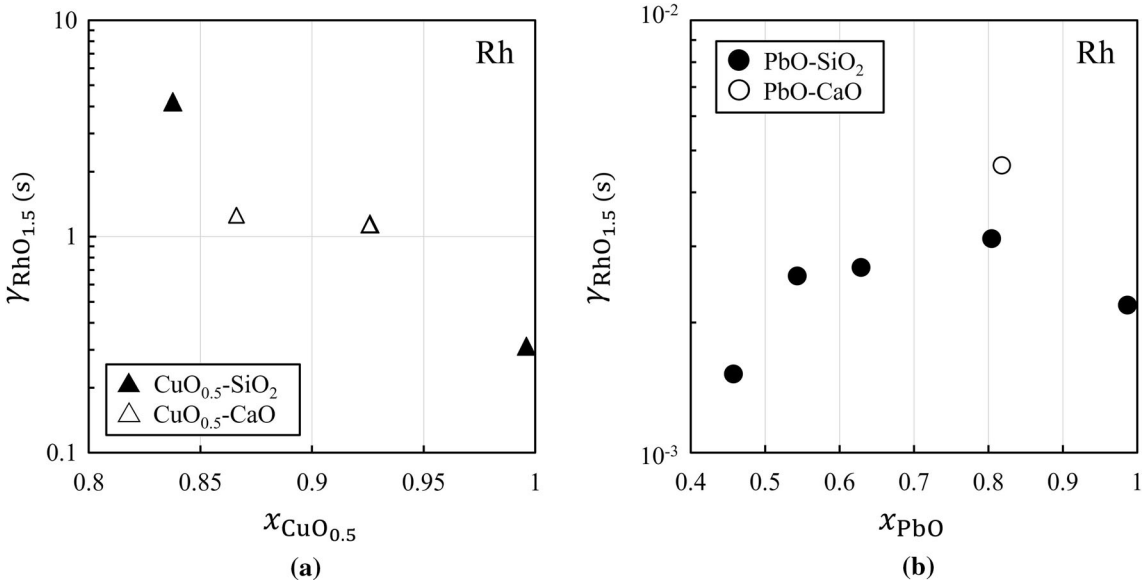

Fig. 9—Activity coefficient of $RhO_{1.5}$ (s) at 1523 K: (*a*) $CuO_{0.5}$–SiO_2 and $CuO_{0.5}$–CaO systems and (*b*) PbO–SiO_2 and PbO–CaO systems.

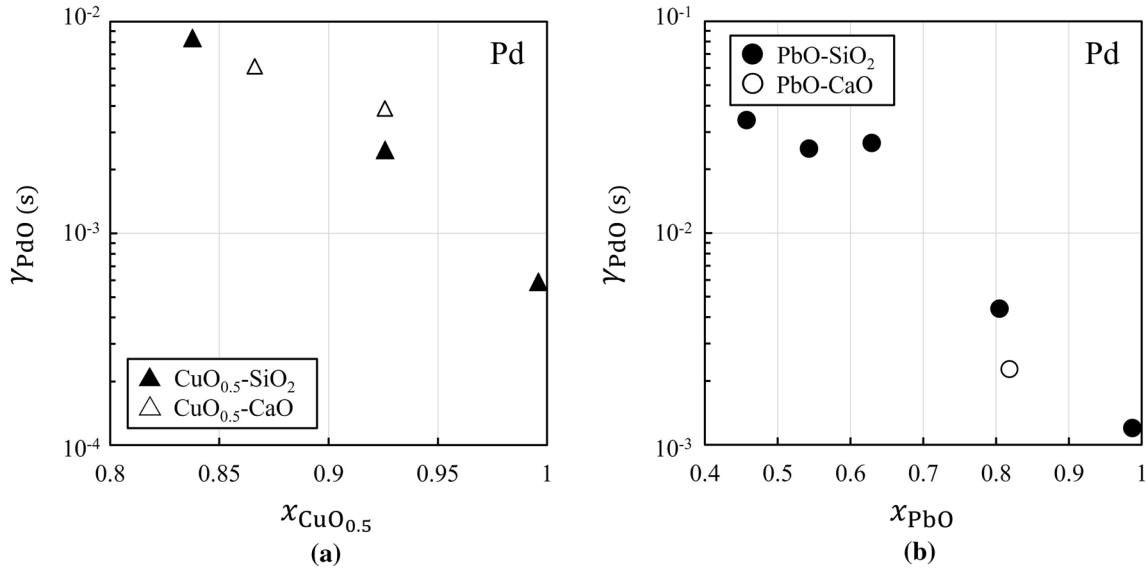

Fig. 10—Activity coefficient of PdO (s) at 1523 K: (*a*) $CuO_{0.5}$–SiO_2 and $CuO_{0.5}$–CaO systems and (*b*) PbO–SiO_2 and PbO–CaO systems.

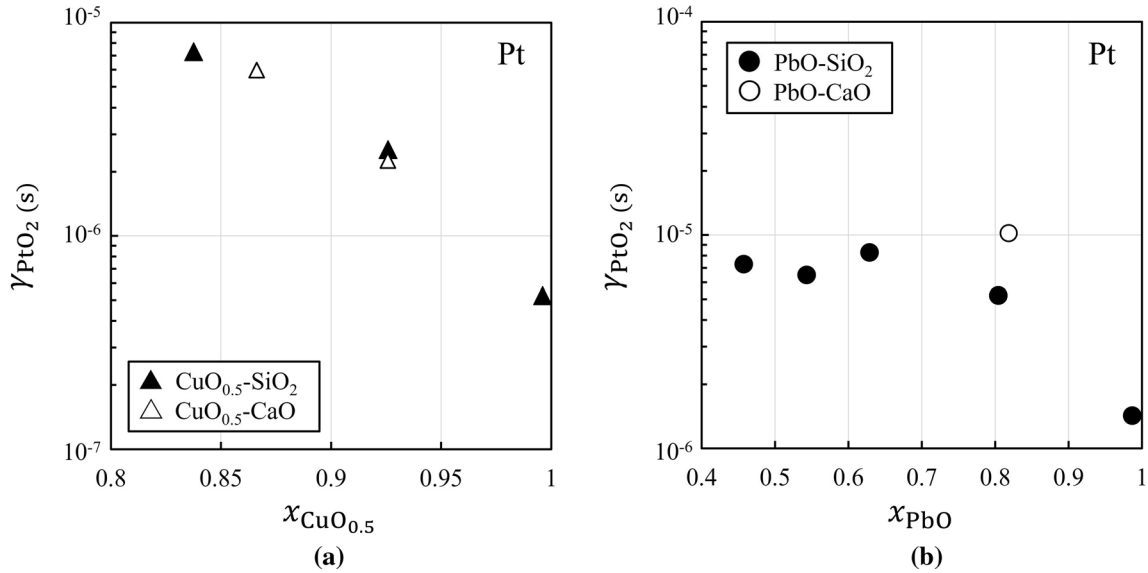

Fig. 11—Activity coefficient of PtO_2 (s) at 1523 K: (*a*) $CuO_{0.5}$–SiO_2 and $CuO_{0.5}$–CaO systems and (*b*) PbO–SiO_2 and PbO–CaO systems.

Therefore, the addition of SiO_2 or CaO could reduce the loss of PGMs in slag during the oxidation smelting process as well as the amount of PGMs circulating in the recycling process.

3. The activity coefficient of each oxide in the slag was calculated, assuming the oxidation states of PGMs in the slag as $RhO_{1.5}$, PdO, and PtO_2. The addition of SiO_2 and CaO significantly changed the activity coefficient of each PGM oxide in the slag.

ACKNOWLEDGMENTS

We would like to thank Editage (www.editage.com) for English language editing.

CONFLICT OF INTEREST

The authors declare that they have no conflict of interest.

REFERENCES

1. T.N. Aleksandrova and C. O'Connor: *J. Min. Inst*., 2020, vol. 244, pp. 462–73.
2. D. Xun, H. Hao, X. Sun, Z. Liu, and F. Zhao: *J. Clean. Prod*., 2020, vol. 266, 121942.
3. Y. Taninouchi and T.H. Okabe: *J. Japan Inst. Met. Mater*., 2021, vol. 85 (8), pp. 294–304.
4. S. Suzuki, M. Ogino, and T. Matsumoto: *J. MMIJ*., 2007, vol. 123(12), pp. 734–36.
5. C. Hagelüken: *Acta Metall. Slovaca*, 2006, vol. 12, pp. 111–20.
6. S. Nakamura and N. Sano: *Metall. Mater. Trans. B*, 1997, vol. 28B, pp. 103–08.
7. S. Nakamura, K. Iwasawa, K. Morita, and N. Sano: *Metall. Mater. Trans. B*, 1998, vol. 29B, pp. 411–14.
8. C. Wiraseranee, T.H. Okabe, and K. Morita: *Metall. Mater. Trans. B*, 2013, vol. 44B, pp. 584–92.
9. C. Wiraseranee, T. Yoshikawa, T.H. Okabe, and K. Morita: *J. Min. Metall. Sect. B*., 2013, vol. 49(2), pp. 131–38.
10. C. Wiraseranee, T. Yoshikawa, T.H. Okabe, and K. Morita: *Mater. Trans*., 2014, vol. 55(7), pp. 1083–090.
11. K. Morita, C. Wiraseranee, H. Shuto, S. Nakamura, K. Iwasawa, T.H. Okabe, and N. Sano: *Miner. Process. Extr. Metall*., 2014, vol. 123(1), pp. 29–34.
12. K. Baba and K. Yamaguchi: *J. MMIJ*, 2013, vol. 129 (5), pp. 208–212.
13. K. Yamaguchi: *Proc. Copper 2013*, Santiago, Chile, 2013, vol. 2013, pp. 775–84.
14. M.A.H. Shuva, M.A. Rhamdhani, G.A. Brooks, S.H. Masood, and M.A. Reuter: *Metall. Mater. Trans. B*, 2016, vol. 48, pp. 317–27.
15. K. Avarmaa, H. Johto, and P. Taskinen: *Metall. Mater. Trans. B*, 2016, vol. 47B, pp. 244–55.
16. K. Avarmaa, L. Klemettinen, H. O'Brien, and P. Taskinen: *Miner. Eng*., 2019, vol. 133, pp. 95–102.
17. L. Klemettinen, K. Avaramaa, H. O'Brien, A. Jokilaakso, and P. Taskinen: *JOM*, 2020, vol. 72(16), pp. 2770–777.
18. M. Chen, K. Avarmaa, L. Klemettinen, H. O'Brien, D. Sukhomlinov, J. Shi, P. Taskinen, and A. Jokilaakso: *Metall. Mater. Trans. B*, 2020, vol. 51B, pp. 1495–508.
19. M. Chen, K. Avarmaa, L. Klemettinen, H. O'Brien, J. Shi, P. Taskinen, D. Lindberg, and A. Jokilaakso: *Metall. Mater. Trans. B*, 2021, vol. 52B, pp. 871–82.
20. A. Borisov and L. Danyushevsky: *Eur. J. Mineral*., 2011, vol. 23(3), pp. 355–67.
21. K. Yamaguchi, H. Sekimoto, T. Kon, A. Ishizaka, T. Yoshida, and T. Honda: *Proc. Eur. Metall. Conference EMC, 2013*, Weimar, Germany, 2013, vol. 2013, pp. 267–76.
22. W. Nishijima and K. Yamaguchi: *J. Japan Inst. Met. Mater*., 2014, vol. 78, no. 7, pp. 267–273.
23. T. Murata, Y. Takahashi, and K. Yamaguchi: *Mater. Trans*., 2022, vol. 64(2), pp. 555–63.
24. D.R. Swinbourne, S. Yan, and S. Salim: *Miner. Process. Extr. Metall*., 2005, vol. 114(1), pp. 23–9.
25. T. Hidayat and E. Jak: *Int. J. Mater. Res*., 2014, vol. 105(3), pp. 249–57.
26. M. Shevchenko and E. Jak: *J. Am. Ceram. Soc*., 2018, vol. 101(1), pp. 458–71.
27. M. Shevchenko and E. Jak: *J. Phase Equilib. Diffus*., 2019, vol. 40, pp. 148–55.
28. M. Shevchenko and E. Jak: *Calphad*, 2020, vol. 70, 101807.
29. C.W. Bale, E. Bélisle, P. Chartrand, S.A. Decterov, G. Eriksson, A.E. Gheribi, K. Hack, I.H. Jung, Y.B. Kang, J. Melançon, A.D. Pelton, S. Petersen, C. Robelin, J. Sangster, P. Spencer, and M-A. Van Ende: *CALPHAD*, 2016, vol. 54, pp. 35–53.
30. A. Roine: *Outokumpu HSC Chemistry for Windows, Chemical Reaction and Equilibrium Software with Extensive Thermochemical Database*, HSC Ver. 6.1, Outokumpu Research Oy, Pori, 2008.
31. Y. Takeda and A. Yazawa: *J. Min. Metall. Inst. Jpn*., 1986, vol. 102, pp. 311–16.
32. K. Okajima and H. Sakao: *Trans. Jpn. Inst. Met*., 1973, vol. 14(1), pp. 68–74.